ELSEVIER

Journal of Nuclear Materials 301 (2002) 170–182

journal of nuclear materials

www.elsevier.com/locate/jnucmat

EPMA and SEM of fuel samples from PWR rods with an average burn-up of around 100 MWd/kgHM

R. Manzel [a], C.T. Walker [b,*]

[a] *Framatome ANP GmbH, P.O. Box 3220, D-91050 Erlangen, Germany*

[b] *European Commission Joint Research Centre, Institute For Transuranium Elements, P.O. Box 2340, D-76125 Karlsruhe, Germany*

Received 3 September 2001; accepted 16 November 2001

Abstract

Samples from the high and low power regions of two fuel rods with average burn-ups of 89.5 and 97.8 MWd/kgHM were examined. Electron probe microanalysis (EPMA) was used to measure the radial distributions of Xe, Cs and Nd in the UO_2 fuel matrix, and scanning electron microscopy (SEM) was used to study the change in the UO_2 microstructure across the fuel pellet radius. EPMA showed that a large fraction of the xenon created had been released from the fuel matrix of the high power samples at all radial positions. In these samples, SEM revealed the presence of recrystallised grains at intermediate radial positions where thermal fission gas release had previously occurred. Evidence of recrystallisation was found throughout the pellet cross-sections of the low power samples. It is concluded that recrystallisation of the fuel grains at intermediate radial positions is mainly responsible for the marked increase in fission gas release to the rod free volume at burn-ups above 80 MWd/kgHM.

1. Introduction

The electrical utilities are continuously striving to increase the burn-up at which nuclear fuel assemblies are discharged from the reactor. The main inducements for this are a reduction in the fuel cycle cost and a decrease in the amount of spent fuel to be reprocessed or stored. Since 1980 the average discharge burn-up of Framatome PWR fuel assemblies of Siemens design has increased in Germany from under 35 to 52 MWd/kgHM (where HM equals mass of U + Pu) and is projected to reach about 70 MWd/kgHM over the next decade [1]. Irradiation of 'pathfinder' fuel rods has shown that this burn-up can be reached with today's standard UO_2. Most importantly, no life limiting effects have been observed during post-irradiation examination even at pellet burn-ups above 100 MWd/kgHM [2].

When the local burn-up reaches about 60 MWd/kgHM [3] the UO_2 grains in the outer region of the fuel pellet begin to recrystallise. This has been attributed to the accumulation of irradiation damage at fuel temperatures below 1200 °C [4,5]. The transformed microstructure, which is referred to as the high burn-up structure, consists of small grains of average size 0.15 μm and a high concentration of pores of typical diameter 1–2 μm [6,7]. Earlier concern that recrystallisation may impose a burn-up limit on UO_2 fuel has not been confirmed. This concern arose from the assumption that as burn-up is increased a point will eventually be reached at which a large fraction of the fission gas that is accumulated in the pores of the high burn-up structure [8–10] will be released to the rod free volume. Such a release could eventually cause thermal feedback effects and could possibly lead to fuel rod over-pressurisation and clad lift-off [11]. Thermal feedback effects refer to the enhancement of fuel swelling and fission gas release that accompanies the rise

* Corresponding author. Tel.: +49-7247 951 477; fax: +49-7247 951 590.

E-mail address: clive.walker@itu.fzk.de (C.T. Walker).

0022-3115/02/$ - see front matter
PII: S0022-3115(01)00753-X

in fuel temperature caused by the accumulation in the fuel-cladding gap of Xe, which has a poor thermal conductivity compared with the fill-gas He.

Since 1993, the Institute for Transuranium Elements and Framatome APN GmbH, formerly Siemens Nuclear Power GmbH, have been co-operating in a study of the performance of PWR fuel at burn-ups beyond 60 MWd/kgHM. The focus of the work is fission gas release and fuel swelling and the contribution that the high burn-up structure makes to these quantities [2,11,12]. The present paper reports electron probe microanalysis (EPMA) and scanning electron microscopy (SEM) results obtained on fuel samples cut from the high and low power regions of two PWR rods with average burn-ups around 100 MWd/kgHM. EPMA was used to measure the radial distributions of the fission products Xe, Cs and Nd in the UO_2 fuel matrix, and SEM was used to study the change in the UO_2 microstructure across the fuel pellet radius. The high burn-up structure is characterised by loss of Xe from the fuel matrix [3]. Therefore, the Xe distribution profile provides information on the radial penetration of the high burn-up structure. Unlike Xe, Cs is completely retained in the high burn-up structure [13], but undergoes thermal release in the central region of the fuel [14].

Moreover, the apparent diffusion coefficients of Xe and Cs are similar at temperatures above that required for thermal restructuring [14,15]. These facts have led Lassmann et al. [15] to propose that the percentage of fission gas released by thermally activated processes in the central region of the fuel will be similar to the level of Cs release derived from the EPMA radial concentration profile. Neodymium, which is immobile in UO_2 nuclear fuel, was used as an indicator of the local burn-up.

The work had three main objectives. First, to obtain further evidence needed to identify the mechanism of formation of the high burn-up structure. Second, to explain why in this series of irradiations, fission gas release was observed to increase substantially above 60 MWd/kgHM, although over the whole period of extended irradiation the fuel temperature was less than 1000 °C. Third, to establish whether an important fraction of the gas released to the rod free volume at extended burn-up originated from the high burn-up structure.

2. Fuel characteristics and irradiation history

The fuel pellet and rod design characteristics are given in Table 1. The rods were of standard PWR design for Siemens built reactors with plenum space above and below the fuel stack. The fuel rod cladding was a highly corrosion resistant zirconium alloy.

The rods were irradiated in Siemens built 15 × 15 fuel assemblies in a commercial PWR reactor. The irradiation of rod 12H3 spanned eight reactor cycles and lasted 2631 effective full power days (EFPD), whereas the irradiation of rod 12C3 spanned nine cycles and lasted 2913 EFPD. The power history and burn-up evolution is shown in Fig. 1. At the end of the fourth irradiation cycle when the original fuel assemblies had reached their nominal discharge burn-up in the region of 60 MWd/kgHM, the rods were transferred to carrier assemblies containing partially burnt fuel for further irradiation. From Fig. 1 it is seen that during the first four cycles the average power rating fell from 34 to 20 kW m^{-1}. After transfer to the carrier assembly, the power rating decreased more gradually from 18 kW m^{-1} in the fifth irradiation cycle to 14 kW m^{-1} in the ninth and final cycle. The rod average burn-up was 89.5 MWd/kgHM for 12H3 and 97.8 MWd/kgHM for 12C3.

Table 1
Fuel pellet and rod design characteristics

Pellet diameter (mm)	9.3
Initial enrichment (wt% ^{235}U)	3.5
Fuel density (%TD)	95
2D grain size [a] (μm)	9–12
Diametrical gap (μm)	160–190
He fill gas pressure (bar)	22.5
Cladding material	Zr-based alloy

[a] Linear intercept.

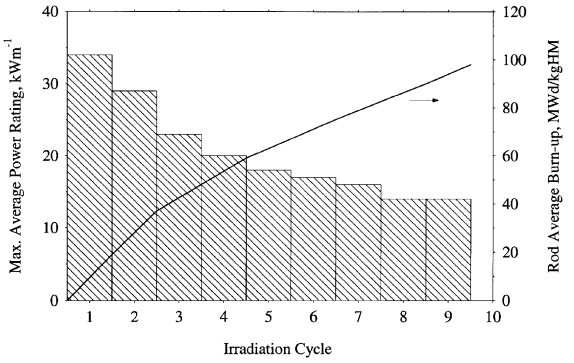

Fig. 1. Power history and burn-up evolution in the fuel rods 12C3 and 12H3. Rod 12H3 was irradiated for eight reactor cycles and rod 12C3 for nine reactor cycles.

The axial burn-up distribution in rod 12C3 as revealed by the gross axial gamma scan is shown in Fig. 2. The gamma scan shows a typical axial profile of a PWR fuel rod. At the top and bottom of the fuel stack the burn-up falls sharply. The axial burn-up distribution in rod 12H3 was very similar to that in rod 12C3.

3. Fuel samples examined by EPMA and SEM

The burn-up and axial position in the rods of the fuel samples examined by EPMA and SEM are given in

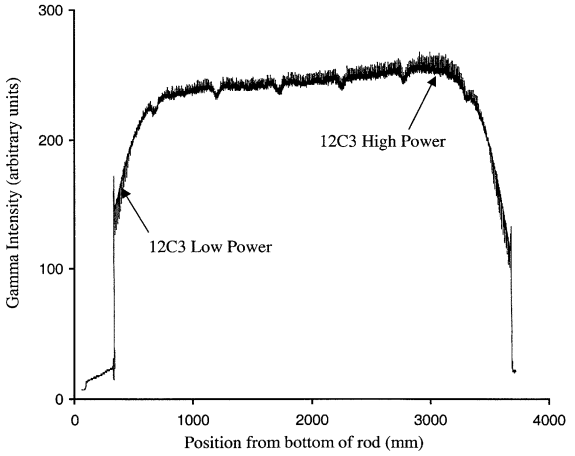

Fig. 2. The gross axial gamma scan for rod 12C3 showing the positions of the high and low power samples. The effect of the spacer grids in lowering the power can clearly be seen.

Table 2. It is seen that the samples were taken from the same axial positions in both rods. The burn-up of the high power samples was around 100 MWd/kgHM, whereas the burn-up of the low power samples was between 60 and 70 MWd/kgM. The burn-up of the high power samples was determined by dissolving adjacent fuel pellets in 6 M nitric acid and determining the ratio between the ^{148}Nd concentration and the U and Pu concentrations in the solution using inductive coupled plasma mass spectrometry (ICP-MS). The burn-up of the low power samples was not determined by chemical burn-up analysis, but was calculated from the ratio of the gamma intensity at the axial positions of the high and low power samples in the gross gamma scans. The position of the high and low power samples are marked on the gross gamma scan in Fig. 2. It can be seen that at the position of the high power sample, intensity peaks at the pellet interfaces reveal that Cs migration has occurred. At the position of the low power sample, the pellet interfaces are marked by pronounced intensity drops showing that little migration of Cs had taken place.

Table 2
Pellet burn-up and axial position in the rods of the fuel samples examined by EPMA and SEM

Sample number	Burn-up (MWd/kgHM)	Axial position (cm)
12C3 (HP)	102	312.0–312.7
12C3 (LP)	69	31.6–32.3
12H3 (HP)	95	312.0–312.7
12H3 (LP)	65	31.6–32.3

HP—high power; LP—low power. The burn-up is derived from chemical burn-up analysis and the axial power profile given by the gross axial gamma scan (see Fig. 1). The axial position is the distance in cm from the bottom of the rod.

In order to interpret correctly the EPMA and SEM results, knowledge of the fuel temperature during the irradiation is required. The fuel rods 12H3 and 12C3 experienced similar power histories and consequently very similar temperatures during their irradiation. Since the two samples were taken from axial positions with markedly different power histories the fuel temperatures varied accordingly.

In the first two irradiation cycles the centre temperature of the high power samples dropped from 1650 to 1150 °C. During the remainder of the irradiation it was in the range 850–950 °C. In the case of the low power samples, apart from at the end of the first cycle when 1000 °C was reached, the fuel centre temperature was between 500 and 600 °C throughout the irradiation. The advanced version of the Framatome ANP fuel rod analysis and design code CARO-E [16] was used to calculate the fuel temperature. This code takes into account the degradation of thermal conductivity of the fuel pellet that occurs with increase in burn-up; both due to build-up of fission products in the UO_2 lattice and the presence of gas filled pores in the high burn-up structure.

4. Other post-irradiation examination results

In addition to SEM and EPMA, numerous other post-irradiation examinations were carried out on rods 12H3 and 12C3 and the high and low power samples. These included rod puncturing and mass spectrometry of the plenum gas, optical microscopy and determination of the fuel density. The results of these examinations have been reported in detail elsewhere (see e.g., Ref. [2]). In this section a summary of the principal findings is given. The fractional fission gas release determined by puncturing was 22% for rod 12H3 and 23.5% for rod 12C3. These are high values compared with the fractional release of 5–10% obtained at rod average burn-ups of 50 MWd/kgHM (Fig. 3). The isotopic composition of the plenum gas in both rods gives a Xe/Kr ratio of 10.8. This ratio is intermediate between the values for gas resulting from the fission of ^{235}U (Xe/Kr = 7) and the fission of ^{239}Pu (Xe/Kr = 19) [17], confirming that Pu fission made an important contribution to the burn-up. Optical microscopy revealed that in the high power samples of rods 12C3 and 12H3 the high burn-up structure had penetrated 1.15 and 0.8 mm, respectively. By comparison, in the low power samples the width of the zone at the pellet surface containing the high burn-up structure was less than 0.2 mm. Thus, the depth of penetration of the high burn-up structure increased dramatically with increase in pellet burn-up from above 65 MWd/kgHM (see Fig. 4).

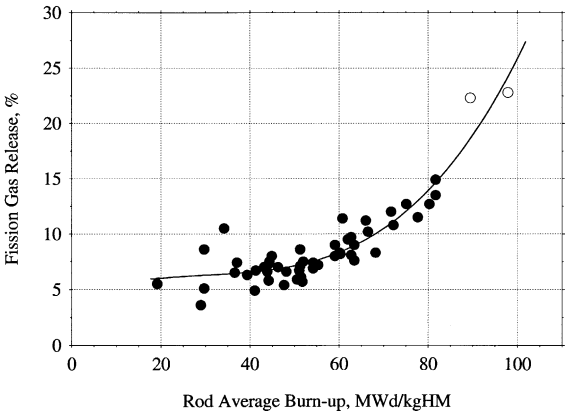

Fig. 3. Puncture results for PWR rods with an average burn-up of 15–100 MWd/kgHM. With increase in burn-up from 50 to 100 MWd/kgHM the percentage of fission gas released to the rod free volume increases from less than 10% to about 25%. The open circles are the data points for rods 12H3 and 12C3.

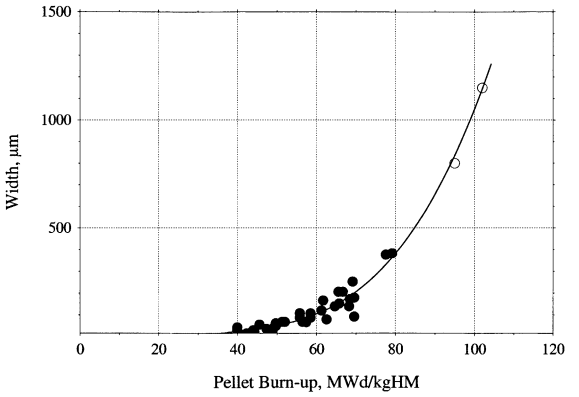

Fig. 4. Optical microscopy results for the penetration depth of the high burn-up structure in PWR fuel. The open circles are the data points for the high power samples from rods 12H3 and 12C3.

Fuel pellet density was measured by immersion in 1,1,2,2-tetrabromoethane. The density of fuel pellets from the high power regions of the rods was 9.67 (12H3) and 9.48 $g\,cm^{-3}$ (12C3), whereas the density of fuel pellets from the low power region of the rods was of the order of 10.0 $g\,cm^{-3}$. The decrease in fuel density above 65 MWd/kgHM represents an increase in the fuel swelling rate from the standard value of 1% per 10 MWd/kgHM, resulting from the replacement of heavy metal atoms by fission product atoms, to 1.5% per 10 MWd/kgHM. This change in swelling rate is attributed to the development of the porous high burn-up structure in the outer region of the fuel.

5. Methods

5.1. Electron probe microanalysis

EPMA was performed on the Institute's microprobe, which is a unique instrument [18]. It combines the high performance crystal spectrometers of the Cameca MS46 analyser with the three lens electron optical column of the CAMEBAX microprobe and is specially shielded with lead and tungsten to permit the analysis of irradiated nuclear fuel.

EPMA of Xe, Cs and Nd was carried out at an electron acceleration potential of 25 kV and a beam current of 250 nA. Xenon was analysed using the $L\alpha_1$ X-ray line and a $10\bar{1}1$ quartz diffracting crystal, Cs using the $L\beta_1$ line and a LiF crystal and Nd using the $L\alpha_1$ line and a LiF crystal. Xenon and Cs were analysed simultaneously and, therefore, at exactly the same location, whereas Nd was analysed separately. The EPMA matrix correction was carried out using the PAP [19] option in the XMAS® X-ray microanalysis program marketed by SAMx, France. For the correction, measured k-values for U and Pu and a fixed oxygen concentration of 11.8 wt% were introduced in the XMAS program.

Xenon was analysed using the procedure developed at the Institute for Transuranium Elements [20]. This involved the use of antimony as a standard for Xe and the application of a correction factor that was derived by interpolating the intensity of pure solid Xe from the intensities for the elements on each side of Xe in the periodic table. For the analysis of Cs, a caesium iodide standard was used. To obtain a stable signal the standard was analysed at a beam current of 50 nA and the acquisition time was restricted to 10 s.

Forty-six data points were used to construct the radial distribution profiles for Xe, Cs and Nd. In the outer region of the fuel, where the high burn-up structure was present, the points were spaced at intervals of 50 μm, with the first point 10 μm from the pellet rim. In the central region of the fuel, the points were spaced further apart at intervals of 150 μm. At each location the concentrations of Xe, Cs and Nd were determined from the average of six peak and three background measurements of 50 s duration. The measurements were made away from grain boundaries in the central region of the fuel, thereby avoiding pores, large gas bubbles and cracks, and away from gas pores in the high burn-up structure. Thus, the concentrations of Xe and Cs reported represent the amounts in solution in the UO_2 lattice and trapped in small gas bubbles smaller than 0.1 μm. The specimen current image (electron absorption image) was used to obtain information about the fuel microstructure at the locations selected for analysis and to position the electron beam.

Immediately prior to EPMA the fuel specimens were polished with oil using standard metallographic

techniques and ion etched for 15 min at a low beam current. To ensure good conductivity, a thin film of aluminium 20 nm thick was applied to the specimen surface by vacuum evaporation.

5.2. Scanning electron microscopy

SEM was performed on a JEOL 6400 scanning electron microscope. The electron column and specimen chamber of the machine are installed in a glove-box inside a steel cell offering irradiation protection. The secondary electron detector is shielded with lead and fitted with an electron spectrometer that filters out the beta-rays emitted by irradiated nuclear fuel samples [21]. The surface to be examined by SEM was prepared by scratch fractography, which involved drawing a stainless steel stylus with a tungsten carbide tip across the fuel diameter. The debris resulting was removed by repeatedly taking cellulose acetate replicas of the specimen surface. When clean, the specimen surface was coated with a thin layer of gold 20–30 nm thick by vacuum evaporation to avoid electron charging effects. The SEM investigation of the fuel microstructure was carried out along the same pellet diameter that had been used for EPMA.

6. EPMA Results

6.1. Radial distribution of xenon

The radial distribution of Xe in the high power samples from rods 12H3 and 12C3 is shown in Fig. 5. It can be seen that in the outer region of the fuel the level of Xe retention was noticeably higher in the high power sample from 12H3 than in the high power sample from 12C3. In the central region of the fuel the concentration of retained Xe was in the range 0.1–0.2 wt% in both samples. As seen from Table 3, the integral average concentration of retained Xe in the samples was 0.30 (12H3) and 0.22 wt% (12C3), which is substantially less than the created amounts of 1.3 and 1.4 wt%.

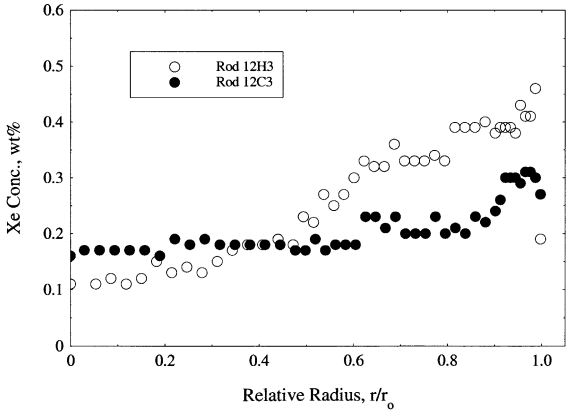

Fig. 5. Radial distribution of Xe in the high power samples from rods 12H3 and 12C3.

Table 3
Integral average concentrations of Xe, Cs and Nd in the samples

Sample	Pellet burn-up (MWd/kgHM)	Concentration (wt%)		
		Xe	Cs	Nd
12C3 (HP)	102	0.22	0.50	1.34
12C3 (LP)	69	0.69	0.47	0.76
12H3 (HP)	95	0.30	0.55	0.98
12H3 (LP)	65	0.82	0.52	0.63

HP—high power; LP—low power.

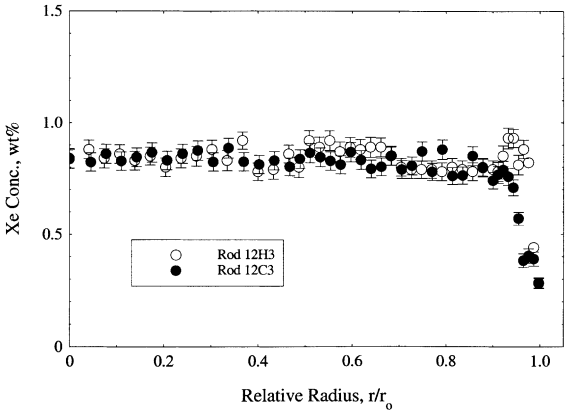

Fig. 6. Radial distribution of Xe in the low power samples from rods 12H3 and 12C3. The error bars mark the confidence limits on the concentrations at a significance level of 99%.

The radial distribution of Xe in the low power samples from rods 12H3 and 12C3 is shown in Fig. 6. Considerably more Xe was measured in the low power samples than in the high power samples, although their burn-up was much lower (69 and 65 MWd/kgHM compared with 95 and 102 MWd/kgHM; see Table 2). As can be seen from Fig. 6, in the low power samples the Xe concentration, which was fairly constant in the central region of the fuel, decreased slightly at $r/r_0 = 0.65$ before droping sharply at the pellet rim.

6.2. Radial distribution of caesium

The radial distribution of Cs in the high power samples from rods 12H3 and 12C3 is shown in Fig. 7. It can be seen that the two profiles are broadly similar in form. In the outer region of the fuel, following an initial

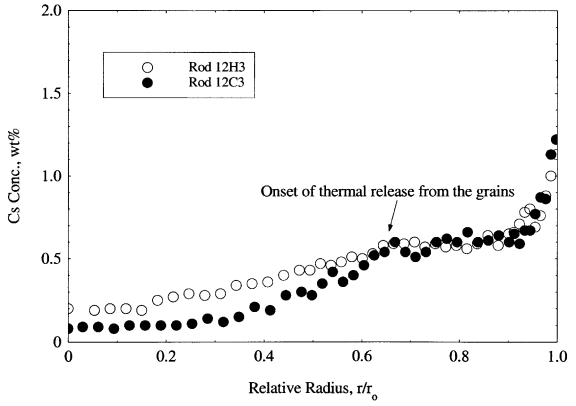

Fig. 7. Radial distribution of Cs in the high power samples from rods 12H3 and 12C3.

sharp decrease, a concentration of around 0.6 wt% Cs is maintained, which approximates to the created amount. In this region the two concentration profiles present an almost perfect match.

In the central region of the fuel, the concentration of retained Cs decreases to 0.1 and 0.2 wt%. The decrease is more gradual in the case of the sample from 12H3, and as a result the integral average concentration of retained Cs reported in Table 3 is slightly higher for this specimen than for the specimen from 12C3.

6.3. Radial distribution of neodymium

The radial distribution of Nd in the high and low power samples from rod 12H3 is shown in Fig. 8. Both profiles are similar in form. In the interior of the fuel the Nd distribution is flat, whereas at the pellet surface the Nd concentration increases steeply due to the fission of Pu created by neutron capture [3,22]. The concentration of Nd at the pellet rim in both samples is about three times higher than the concentration measured in the interior of the fuel.

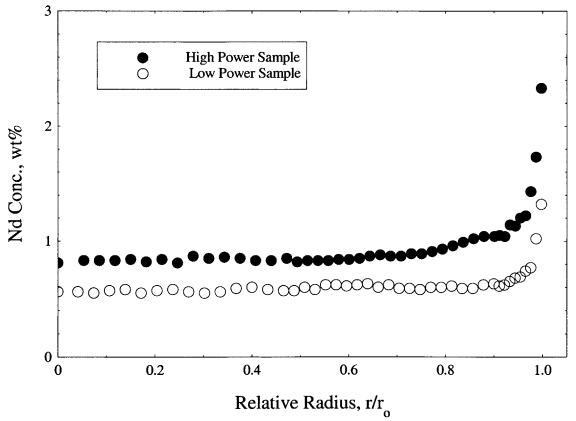

Fig. 8. Radial distribution of Nd in the high and low power samples from rod 12H3.

The integral average concentrations of Nd in the fuel samples are reported in Table 3. It can be seen that a direct correlation between the pellet burn-up and the measured Nd concentration does not exist. There are two main reasons for the lack of correlation. First, the burn-up of the high power samples is mainly the result of ^{239}Pu fission, whereas the burn-up of the low power samples is mainly the result of ^{235}U fission. Second, the quantity of ^{144}Nd resulting from the decay of ^{144}Ce (half-life 284.8 days) is different in the two rods due to differences in the duration of the irradiation and the cooling time before EPMA was performed. Estimation of the amount of Nd created in a given burn-up interval is further complicated by the fact that the neutron spectrum changed continuously throughout the period of extended irradiation because the carrier assembly was inserted in a core of fuel rods of lower burn-up at the beginning of each new irradiation cycle.

7. Scanning electron microscopy results

7.1. Microstructure of the high power samples

The microstructure of the high power sample from rod 12C3 is shown in Fig. 9. It is seen that at $r/r_0 = 0.66$ the UO_2 grains are fully recrystallised. From the Cs profiles in Fig. 7, this position is close to that at which the results of thermally driven processes were first encountered in the fuel. In the interval between $r/r_0 = 0.66$ and the fuel rim the gas pores, which are a feature of the high burn-up structure, clearly increased in size and number. Indeed, the pores at the rim of the pellet are extremely large compared with those 200 μm further in. It is evident from the appearance of the pores at the pellet rim that many of them had experienced coalescence. This, however, had not been sufficient to result in the formation of gas release channels.

The first unequivocal signs of grain sub-division were detected at around $r/r_0 = 0.48$, which is well inside the region where thermal release of Xe and Cs had occurred from the fuel grains (see Fig. 7). It can be seen from Fig. 9, that in the region $r/r_0 = 0.52$–0.60 the fuel microstructure was a mixture of untransformed and recrystallised UO_2 grains. The untransformed grains are characterised by the transgranular mode of fracture. A number of pores are seen in the micrograph showing the microstructure of the fuel in the region $r/r_0 = 0.52$–0.60. These do not show the facetted morphology exhibited by the gas pores of the high burn-up structure (cf. the pore morphology at $r/r_0 = 0.70$–0.95). In the central region of the pellet, grain growth had occurred. The fuel ex-

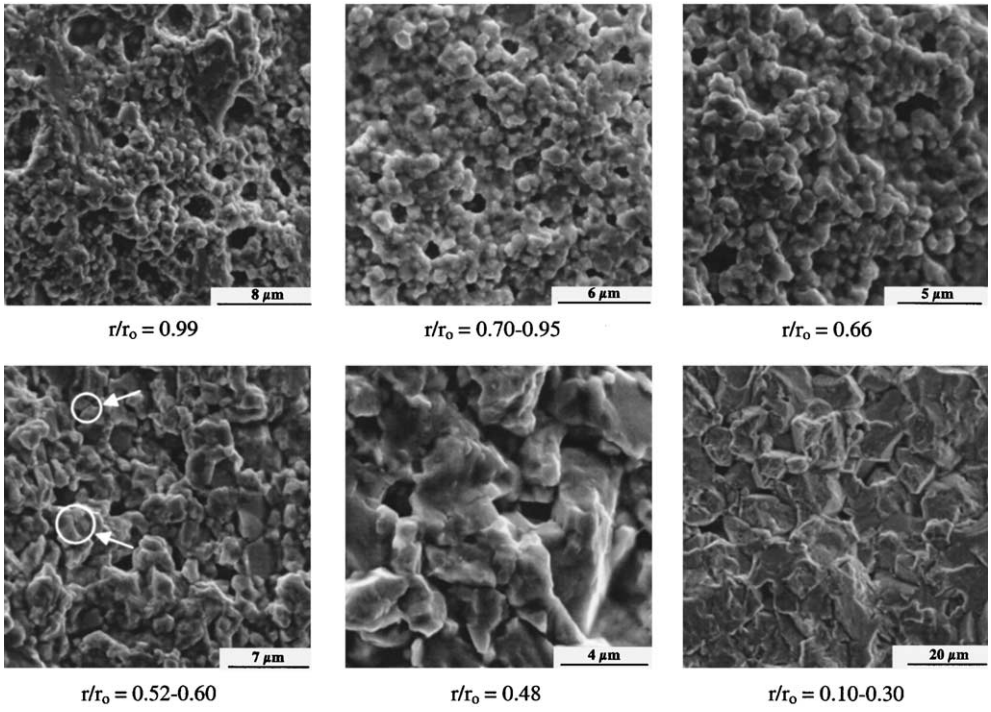

Fig. 9. SEM micrographs showing the microstructure of the fuel at different radial positions in the high power sample from rod 12C3. The white circles enclose grain boundaries that show pearl necklace type gas bubble arrays.

hibited equi-axed grains up to 20 μm in size and the predominant mode of fracture was transgranular. No evidence for recrystallisation was found.

Fig. 10 shows the high burn-up structure in the high power sample from rod 12H3 at $r/r_0 = 0.85$ and on the surface of a crack, exposed by chance, in the same region. Attention is drawn to the fact that far fewer gas pores are present on the crack face.

The microstructure of the high burn-up sample from rod 12H3 was broadly similar to that of the high power

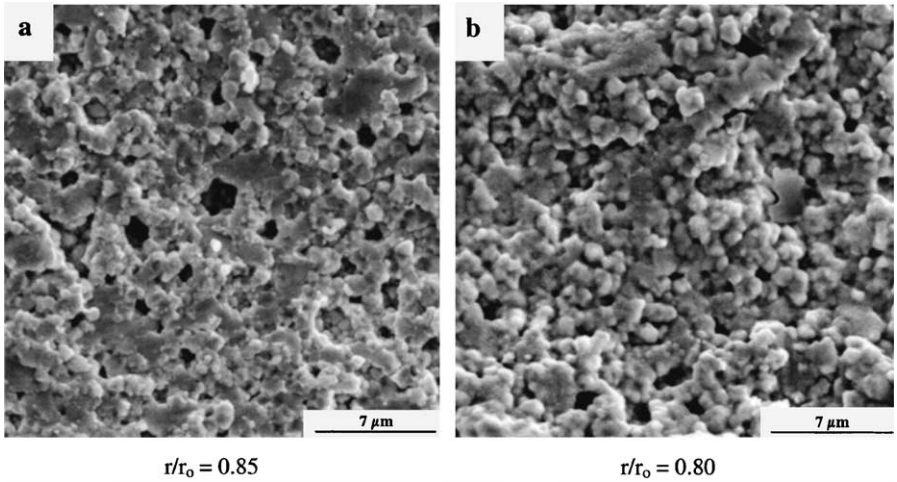

Fig. 10. SEM micrographs of the high burn-up structure in the high power sample from rod 12H3: (a) microstructure at $r/r_0 = 0.85$ and (b) at the surface of a crack in the same region.

sample from rod 12C3. The main difference between the two samples was that in the outer region of the sample from rod 12H3 considerably more grains in the high burn-up structure exhibited transgranular fracture (cf. micrograph a, Fig. 10 with the microstructure at $r/r_0 = 0.70$–0.95 in Fig. 9).

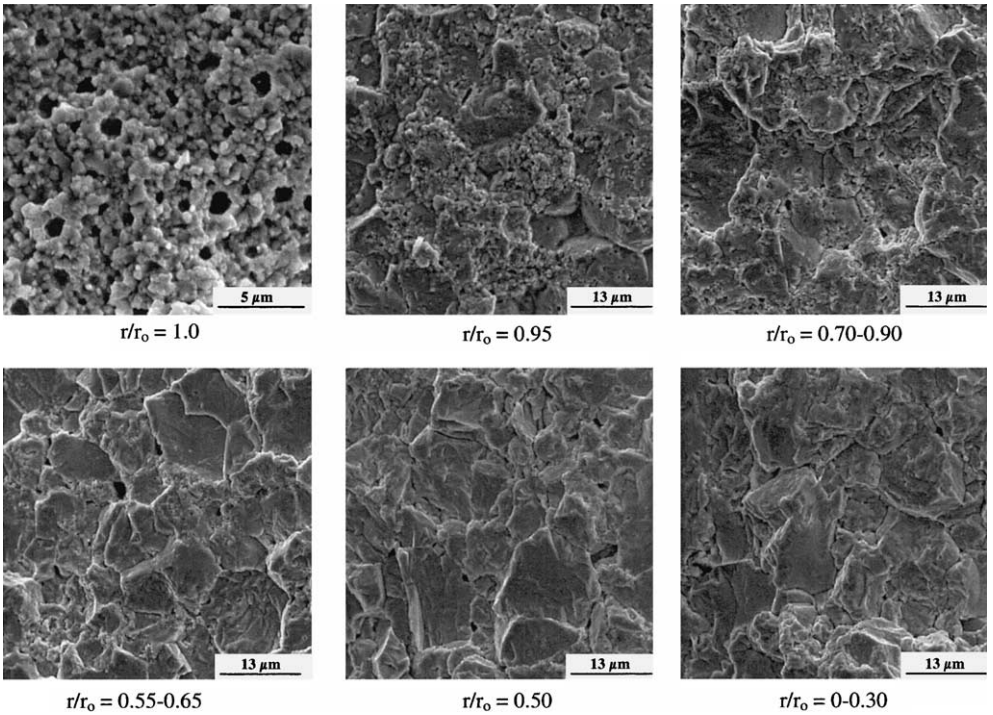

Fig. 11. SEM micrographs showing the microstructure of the fuel at different radial positions in the low power sample from 12C3.

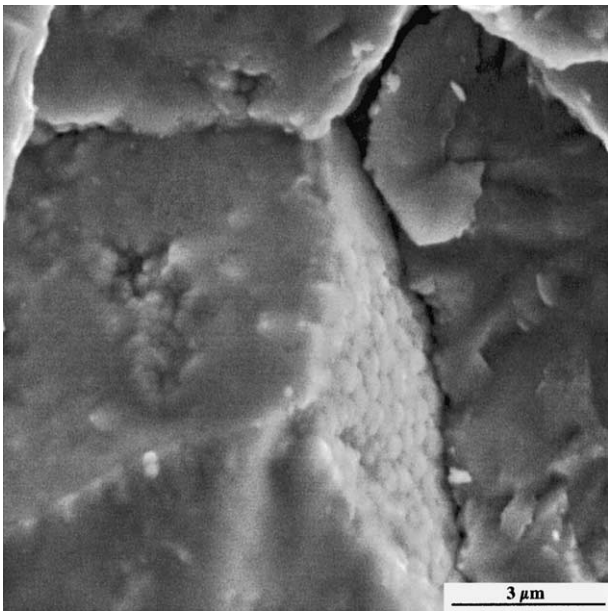

Fig. 12. SEM micrograph showing areas of recrystallisation on the faces of a grain at $r/r_0 = 0.86$ in the low power sample from 12H3. The vertical face is covered by new convex sub-grains, whereas on the horizontal face the process of recrystallisation is just beginning.

7.2. Microstructure of the low power samples

Evidence of grain sub-division was found over the entire pellet cross-sections of the low power samples. The microstructure of the low power sample from rod 12C3 is shown in Fig. 11. It is seen that at the fuel rim the UO_2 grains had completely recrystallised. In the region between $r/r_0 = 0.55$ and $r/r_0 = 0.95$ bands of high burn-up structure run through the microstructure. Between $r/r_0 = 0.55$ and 0.65 the recystallised areas are seen to be confined to grain boundaries and do not exhibit gas pores. Closer to the pellet rim in the region between $r/r_0 = 0.7$ and 0.95, recrystallisation becomes more pronounced and the size of the affected areas increases. At around $r/r_0 = 0.7$, gas pores are first detected in the recrystallised regions along the grain boundaries.

In the central region of the fuel, between $r/r_0 = 0.50$ and the pellet centre the sample exhibits a mixture of intergranular and transgranular fracture. Where intergranular fracture predominated many of the exposed grain faces presented areas of incipient recrystallisation. Moreover, some of them exhibited micron size craters caused by single sub-grains being torn from the grain faces by the tool used to make the scratch.

The low power sample from rod 12H3 exhibited very similar microstructure changes. Fig. 12 shows grain faces decorated with recrystallised areas at $r/r_0 = 0.86$ in that sample. The vertical face of the grain featured in the micrograph is almost completely covered with new convex sub-grains, whereas a single cluster of new subgrains has formed on the horizontal face of the grain.

8. Discussion

8.1. Role of recrystallisation in fission gas release at high burn-up

Probably the most intriguing finding made in the series of irradiations to which the rods 12H3 and 12C3 belong is that although after the second cycle the fuel centre temperature remained around 900 °C the percentage of fission gas released to the rod free volume increased markedly from 5–10% to about 25% (Fig. 3). This is attributed to a progressive increase in the amount of fission gas released from the interior of the fuel in the interval between the pellet centre and $r/r_0 = 0.7$ [2]. The increase in fission gas inventory with burn-up clearly constitutes an important factor in the increase of release from this region. The effect of this is most pronounced in the central region of the fuel where, above a pellet burn-up of 50 MWd/kgHM, the concentration of retained Xe is consistently in the range 0.1–0.3 wt% (see e.g., Fig. 5 in this paper and Fig. 2 in Ref. [2]). Thus, with increase in pellet burn-up from 50 to 100 MWd/kgHM, local release in the region between the pellet centre and $r/r_0 = 0.4$ increased by about two-fifths from about 60 to 85%. The fact that gas retention in the central region of the fuel did not increase significantly above 50 MWd/kgHM implies that throughout the irradiation, gas release channels, which formed on the grain boundaries during the first two reactor cycles, remained open during the period of extended irradiation. It also implies that the local temperature was sufficient to support fast diffusion of gas atoms to the grain boundaries.

With distance from the pellet centre the diffusion rate decreases due to the decrease in fuel temperature. Consequently, in the radial interval between $r/r_0 = 0.4$ and 0.7 the concentration of Xe retained in the grains normally increases and the percentage release decreases. If at $r/r_0 = 0.7$ the local burn-up does not reach the threshold value for the formation of the high burn-up structure, which is around 60 MWd/kgHM [3], complete retention is measured by EPMA at this position. If, however, the local burn-up at $r/r_0 = 0.7$ exceeds the threshold value for the formation of the high burn-up structure, the concentration of Xe measured by EPMA depends on the degree to which the microstructure has transformed and decreases markedly with increase in the local burn-up. The fall in the measured Xe concentration is generally accepted to be due to the transfer of the gas from the UO_2 grains where it can be measured by EPMA to the pores of the high burn-up structure where it is not detected during analysis [3,8]. It was recognised early on, however, that the depth of penetration of the high burn-up structure in the fuel depends not only on burn-up, but also on temperature [23]. In the sense that even when the local burn-up is substantially higher than 60 MWd/kgHM, the high burn-up structure will not form if the fuel temperature is above 1000 °C, because at such temperatures thermal restructuring and thermal fission gas release predominate. Since the burn-up increases with dwell time in the reactor whereas the fuel temperature decreases, recrystallisation will eventually occur in the zone where thermally activated release has occurred early in life. The EPMA and SEM results reported for the high power sample from rod 12C3 in Sections 6 and 7 of this paper substantiate this. Though the extent of the central zone of thermal release cannot be ascertained from the EPMA Xe profile due to the large percentage of gas released from the fuel grains (see Fig. 5), it can be seen from the EPMA Cs profile in Fig. 7 that thermal release had occurred in the region between the fuel centre and $r/r_0 = 0.65$. Grain sub-division is clearly evident in the SEM micrograph in Fig. 9 showing the microstructure of the fuel at $r/r_0 = 0.48$, which is well inside the zone of thermal release. At this radial position, the threshold burn-up for recrystallisation was definitely exceeded during the sixth cycle at which time the local fuel temperature had fallen to 800–850 °C. Thus, it would seem that at the mid-radial position the UO_2 grains

began to recrystallise at the earliest during the sixth cycle and that once begun, their transformation continued during the whole period of extended irradiation. Comparison of the EPMA profiles in Fig. 5 reveals that concentration of retained Xe in the outer region of the fuel continued to decrease during the ninth cycle. Moreover, the SEM investigations on the high power samples revealed that the gas pores at the pellet rim had grown remarkably during the ninth cycle (see Fig. 9). Both findings indicate that the high burn-up structure was still evolving at pellet burn-up around 100 MWd/kgM.

Recrystallisation at intermediate radial positions will result in a resurgence of gas release from the interior of the fuel grains to the grain boundaries in this region late in life. The degree to which the release rate is increased will depend on the volume fraction of the microstructure that has transformed, the size distribution of the recrystallised grains and the local fuel temperature. The release fractions for one year quoted in Table 4 exemplify the level of release enhancement that can be expected at the mid-radial position when the microstructure is completely transformed. Fractional release values are listed for three grains sizes; 10 μm representing the as-fabricated fuel grain size, and 2 and 0.5 μm, representing the recrystallised grain size. The fractional release values given in Table 4 suggest that recrystallisation at the mid-radial position could result in up to a tenfold increase in the percentage of fission gas released from the UO_2 grains to the grain boundaries. It can be seen that the fractional release from 0.5 μm size grains is 0.89 and that the release from 2 μm grains is 0.38. In comparison, the fractional release from 10 μm grains prior to recrystallisation is 0.09.

The fractional release values reported in Table 4 were calculated using the mathematical solution to the equivalent sphere model of Booth that is applicable to in-pile release of stable fission gas isotopes and which takes into account the production rate of the gas [24].

$$f = 1 - \frac{6a^2}{90D^*_{Xe}t} + \frac{6a^2}{\pi^4 D^*_{Xe}t}\sum_{n=1}^{\infty}\frac{1}{n^4}\exp\left(-\frac{n^2\pi^2 D^*_{Xe}t}{a^2}\right), \quad (1)$$

where f is the fractional release, D^*_{Xe} is the apparent diffusion coefficient of Xe, t is the time and a is the radius of the UO_2 grains. D^*_{Xe} was calculated using the equation of Matzke for athermal diffusion; that is, radiation-enhanced diffusion, below 1000 °C [25].

$$D^*_{Xe} = A\dot{F}, \quad (2)$$

where $A = 1.2 \times 10^{-30}$ cm^5 and $\dot{F}$ is the fission rate. For this quantity a typical value of 10^{13} cm^{-3} s^{-1} was taken. This gives a value of 1.2×10^{-21} m^2 s^{-1} for D^*_{Xe}, which is about two orders of magnitude higher than the thermal diffusion coefficient at 800 °C.

For $f \geqslant 0.57$ ($\pi^2 D^*_{Xe}t/a^2 \geqslant 1$) the infinite series converges rapidly and Eq. (1) becomes

$$f = 1 - \frac{6a^2}{90D^*_{Xe}t} + \frac{6a^2}{\pi^4 D^*_{Xe}t}\exp\left(-\frac{\pi^2 D^*_{Xe}t}{a^2}\right). \quad (3)$$

In contrast, for $f \geqslant 0.57$ ($\pi^2 D^*_{Xe}t/a^2 \leqslant 1$), the series does not converge. In this case the following approximation is used:

$$f = 4\sqrt{\frac{D^*_{Xe}t}{\pi a^2}} - \frac{3D^*_{Xe}t}{2a^2}. \quad (4)$$

The fractional release given by Eqs. (3) and (4) is the ratio of the total quantity of gas released by a fuel grain of given diameter in a time interval, t, to the total amount of gas produced by irradiation in that time period.

From EPMA and X-ray fluorescence analysis (XRF) studies on transient-tested fuel (see e.g., [26]) it is known that not all the gas released from the UO_2 grains at intermediate radial positions reaches the rod free volume. A considerable fraction is retained on the grain boundaries in this region of the fuel because gas bubble interlinkage on the grain boundaries and the formation of escape tunnels at grain edges is incomplete. Thus, it is likely that only part of the gas released from the recrystallised grains at intermediate radial positions in the high power samples from rods 12C3 and 12H3 actually escaped to the rod free volume. A certain fraction will be retained on the grain boundaries. In support of this assumption stringers of gas bubbles were observed on some grain boundaries at $r/r_0 = 0.53$ in the high power sample from rod 12C3 and gas escape channels were present throughout the microstructure at this position (see Fig. 9).

It is evident from Fig. 9 that in the high power sample from rod 12C3 the high burn-up structure occupied the entire outer region of the fuel from the pellet surface to $r/r_0 = 0.66$. In this region the local Xe concentration measured by EPMA was 0.2–0.3 wt%. If all of the missing gas is assumed to have been released to the rod free volume, then the average integral release for the pellet cross-section, including release from the central region of the fuel, jumps from around 20%, which is consistent with the rod puncturing result, to about 85%.

Table 4
Fractional release of fission gas during 1 year at a temperature below 1000° C as a function of grain size as given by Eq. (1)

D_{Xe} (m^2 s^{-1})[a]	Fractional release		
	10 μm	2 μm	0.5 μm
1.2×10^{-21}	0.09	0.38	0.89

[a] Calculated using the equation of Matzke for athermal diffusion (Ref. [25]).

Such a high release value is impossible and hence it is assumed that most of the gas released from the recrystallised grains of the high burn-up structure is trapped in the discrete 1–2 μm size pores that pervade the structure. The available experimental evidence supports this view. For example, early investigations using XRF [27] and micro-coring [9] on UO_2 pellets with burn-ups of 45 to 55 MWd/kgHM in which the high burn-up structure was restricted to the pellet rim indicated that the fission gas was completely retained in the structure. Subsequent investigations of pellets with burn-ups above 60 MWd/kgHM using XRF [28] and by the dissolution of fuel samples in a molten salt mixture [29] indicated that 20–30% of the fission gas inventory was released from the high burn-up structure. In the fuel samples studied the high burn-up structure penetrated deep into the fuel.

8.2. Sequence of events in the formation of the high burn-up structure

Spino et al. [30] have proposed that the formation of the high burn-up structure is a consequence of the following sequence of events which unfold as the local burn-up increases. Migration of fission gas out of the UO_2 lattice, the formation of facetted gas pores, over-pressurisation of the pores, grain sub-division around the pores due to the local build-up of mechanical stress. Nogita and Une [5] present a transmission electron microscopy micrograph showing that the density of dislocations at the surface of the gas pores is extremely high, which would indeed suggest that they contain fission gas at high pressure. Nevertheless, they propose a different formation mechanism for the high burn-up structure [5]. In their perception of events, the accumulation of irradiation damage leads to the formation of dislocation tangles, with increasing burn-up these unravel to produce sub-divided grains and those with high-angle boundaries act as nuclei for recrystallisation. Concurrently, nanometer size intragranular fission gas bubbles form by the clustering of vacancies and the capture of fission gas atoms. When recrystallisation occurs these bubbles are swept to the grain boundaries where a small number on preferred sites develop into facetted gas pores.

The observations reported in the present paper indicate that the scenario of Spino et al. [30] and Nogita and Une [5] are to some degree both correct. It is clearly seen from Fig. 11 that the areas of recrystallisation which run through the microstructure of the low power sample from rod 12C3 do not show any gas pores when they are first discerned in the region $r/r_0 = 0.55$–0.65. Gas pores initially appear in the recrystallised areas at around $r/r_0 = 0.70$ and evidently grow in size and increase in number as the transformation of the microstructure proceeds. This indicates that the pores in these areas mainly result from the accumulation of gas released from the recrystallised grains as proposed by Nogita and Une. It is inferred from this that most of the gas pores in the fully developed high burn-up structure formed after the process of recrystallisation had begun. This is supported by the observation that noticeably fewer pores formed in the high burn-up structure in the vicinity of a crack (see Fig. 10). Clearly, cracks provide an infinite sink for the gas that is swept out of the UO_2 grains during recrystallisation and subsequently diffuses out of the recrystallised grains. As a consequence, pore formation is greatly reduced.

Close inspection of the SEM micrographs in Fig. 11 reveals that the UO_2 grains in the region $r/r_0 = 0.7$–95 exhibit a population of micropores. Such pores were not present in the fuel between $r/r_0 = 0.7$ and the pellet centre. It is therefore assumed that their presence is associated with the build-up of irradiation damage in the UO_2 lattice at low temperature and that they are the result of vacancy clustering. From the Nd profile for the low power sample of rod 12H3 in Fig. 8 it can be seen that the burn-up did not increase significantly in the region between the pellet centre and $r/r_0 = 0.9$. Thus, the pores are not the result of an increase in fission gas inventory. It is seen from Fig. 11 that these micropores act as nucleation sites for recrystallisation away from the areas of recrystallisation that had developed earlier in the irradiation. The pores, however, are not the only nucleation sites in this region. As can be seen from Fig. 12, grain boundaries also constitute important nucleation sites. According to Spino et al. [6] the pores that act as nucleation sites contain fission gas at high pressure. Nogita and Une [5] in contrast state that the pores become over-pressurised during coarsening, when they behave as sinks for the gas that is released by the surrounding recrystallised grains. The fact that grain boundaries and pores act simultaneously as nucleation sites in the same region of the fuel suggests that the presence of a free surface is the main criterion for nucleation.

As to the question of whether fission gas release occurs in advance of grain sub-division, no clear evidence for this was found in the fuels investigated in this work. As can be seen from Fig. 6, the EPMA Xe profile for the low power samples drop slightly at around $r/r_0 = 0.65$ before decreasing sharply at about $r/r_0 = 0.95$. Inspection of the SEM micrographs in Fig. 11 reveals that $r/r_0 = 0.65$ roughly corresponds to the onset of the transition zone, where recrystallised and un-recrystallised grains co-exist, and $r/r_0 = 0.95$ approximates to the position where the transformation of the microstructure is complete. It is to be noted that in the central region of the low power fuel samples similar Xe concentrations were measured, although the burn-up of the sample from rod 12C3 is 6% higher than that of the sample from rod 12H3. A possible explanation is that

more gas has been released from the fuel grains in the sample from rod 12C3 because the volume fraction of fuel that has recrystallised is higher.

On the basis of the observations reported in this paper an updated scenario for the sequence of events leading to the formation of the high burn-up structure is presented below. Three principal steps have been identified in the development of the high burn-up structure. These represent the processes that occur with increase in local burn-up from 60 to 300 MWd/kgHM. No observations are available for burn-ups above 300 MWd/kgHM:

Step 1: Nucleation of recrystallised grains at grain boundaries and micropores.

Step 2: Formation of facetted pores in the recrystallised microstructure as a result of diffusion of fission gas out of the new grain structure.

Step 3: Growth of the facetted pores with increase in burn-up as they collect the gas that continuously flows from the surrounding recrystallised grains.

It is unclear whether gas release occurs from the fuel matrix during the actual process of recrystallisation. Nogita and Une [5] have shown that prior to recrystallisation the fuel grains contain a high density of nanometer size gas bubbles, which are absent after grain sub-division has occurred. Bremier et al. [31] have calculated that at the temperature of the pellet rim, 400 °C, radiation-enhanced diffusion can result in the release of large fractions of fission gas from the recrystallised grains in a single reactor cycle. At the same time, they found [32] that for an un-recrystallised grain of diameter 10 μm, it requires 572 days to obtain a fractional release of 0.01 using an apparent diffusion coefficient of 10^{-23} $m^2 s^{-1}$. This is the diffusion coefficient that gives the equilibrium Xe concentration of 0.2–0.3 wt% measured by EPMA in the grains of the high burn-up structure [3]. It appears from these findings that significant gas release from the fuel matrix occurs during recrystallisation and from the recrystallised grains, but not before.

Attention is drawn to the fact that the sequence of events postulated by Spino et al. [30] were formulated on the basis of SEM and EPMA results obtained on a highly enriched (^{235}U, 8.65%) large grain (~20 μm) UO_2 test fuel irradiated in the BR3 reactor. Because of their larger size, the surface to volume ratio of the grains (S/V) in this test fuel was half that of the grains of the PWR fuel investigated in this work (3.0×10^3 cm^{-1} compared with 6.0×10^3 cm^{-1}). This could explain why gas pores were seen to be the primary nucleation sites for grain sub-division in the test fuel, rather than grain boundaries. Walker, who performed the EPMA on the fuel, found no evidence for the release of fission gas from the fuel matrix in advance of grain sub-division and recrystallisation [13].

9. Conclusions

With increase in the rod average burn-up from 50 to 100 MWd/kgHM, fission gas release from the PWR fuel investigated increased by a factor of three from 8% to around 25%. Fission gas release in the interior of the fuel between about $r/r_0 = 0.7$ and the pellet centre was mainly responsible for the increase in release. In the central region of the fuel, gas release channels on the grain boundaries remained open throughout irradiation and the local temperature was sufficient to support fast volume diffusion of gas atoms. Consequently, in this region, all the fission gas created during the period of extended irradiation (four and five reactor cycles) was released to the rod free volume.

In the region $r/r_0 = 0.4$–0.7, a marked increase in fission gas release from the fuel matrix occurred at extended burn-up due to grain sub-division. In this region, thermal fission gas release had occurred at some point during the first four reactor cycles, but prior to recrystallisation, release had almost ceased as a result of a decrease in the local temperature as the irradiation proceeded. The degree by which fission gas release at intermediate radial positions is increased as a result of recrystallisation will depend on the volume fraction of the microstructure that has transformed, the size distribution of the recrystallised grains and the local fuel temperature. Locally, up to a tenfold increase in release from the fuel matrix may be possible. The fraction of this gas that actually escapes to the rod free volume will depend on to extent to which gas release channels are present at the grain boundaries.

Below a burn-up of 80 MWd/kgHM, the increase in gas release to rod free volume is mainly a result of progressive thermal release in the central region of the fuel and the expansion of the zone of thermal release with burn-up. The steep increase in release to the rod free volume above 80 MWd/kgHM is mainly due to an acceleration in the fission gas release rate at the intermediate radial positions between $r/r_0 = 0.4$ and 0.66 caused by recrystallisation of the fuel grains.

In the outer region of the fuel between the pellet surface and $r/r_0 = 0.7$ a large fraction of the gas released from the recrystallised grains of the high burn-up structure is retained in the pore population. At a pellet burn-up of 100 MWd/kgHM the high burn-up structure is still evolving with the growth and coalescence of gas pores and further decrease in the fission gas content of the fuel matrix.

From the SEM and EPMA investigations of the low power samples it is concluded that the facetted pores that are a characteristic feature of the high burn-up structure form during and after recrystallisation in response to fission gas release from the fuel matrix. Diffusion of fission gas out of the fuel matrix prior to recrystallisation is restricted to the immediate surface of

the grains and is insignificant. Grain boundaries and micropores act as nucleation sites for recrystallisation.

Acknowledgements

The work presented in this paper is part of a high burn-up programme being performed by Framatome ANP GmbH in close co-operation with a Swiss utility. Their continuous support is gratefully acknowledged.

References

[1] A. Van de Velde, F. Burtak, Atomwirtshaft 45 (2000) 674.
[2] R. Manzel, C.T. Walker, Proceedings of the ANS International Topical Meeting on LWR Fuel Performance, ANS, La Grange Park, IL, 2000, p. 604.
[3] K. Lassmann, C.T. Walker, J. van de Laar, F. Lindström, J. Nucl. Mater. 226 (1995) 1.
[4] C.T. Walker, Concerning the microstructure changes that occur at the surface of UO_2 pellets on irradiation to high burn-up, European Commission, Institute for Transuranium Elements, Karlsruhe, Germany, Report K0291141 (1991).
[5] K. Nogita, K. Une, J. Nucl. Mater. 226 (1995) 302.
[6] J. Spino, K. Vennix, M. Coquerelle, J. Nucl. Mater. 231 (1996) 179.
[7] I.L.F. Ray, Hj. Matzke, H.A. Thiele, M. Kinoshita, J. Nucl. Mater. 245 (1997) 115.
[8] M.E. Cunningham, M.D. Freshley, D.D. Lanning, J. Nucl. Mater. 188 (1992) 19.
[9] R. Manzel, R. Eberle, Proceedings of the International Topical Meeting on Light Water Reactor Fuel Performance: Fuel for the 90s, Avignon, France 1991, vol. 11, ANS/ENS, 1991, p. 528.
[10] K. Nogoita, K. Une, Nucl. Instrum. Meth. B 141 (1998) 481.
[11] R. Manzel, M. Coquerelle, M.R. Billaux, Proceedings of the ANS International Topical Meeting on LWR Fuel Performance, ANS, La Grange Park, IL, 1994, p. 335.
[12] R. Manzel, M. Coquerelle, Proceedings of the ANS International Topical Meeting on LWR Fuel Performance, ANS, La Grange Park, IL, 1977, p. 463.
[13] C.T. Walker, J. Nucl. Mater. 275 (1999) 56.
[14] C.T. Walker, C. Bagger, M. Mogensen, J. Nucl. Mater. 240 (1996) 32.
[15] K. Lassmann, A. Schubert, J. van de Laar, C.T. Walker, Proceedings of the International Seminar on Fission Gas Behaviour in Water Reactor Fuels, Cadarache, France, Les Journees de Cadarache, 26–29 Sept. 2000, NEA/NCS/DOC (2000) 20.
[16] F. Sontheimer, H. Landkron, IAEA Tech. Committee Meeting on Nuclear Fuel Behaviour at High Burn-up and its Experimental Support, Windermere, UK, June 2000, IAEA-TECDOC-1233 (2001) p. 105.
[17] R.J. White, S.B. Fisher, P.M.A. Cook, R. Stratton, C.T. Walker, I.D. Palmer, J. Nucl. Mater. 288 (2001) 43.
[18] C.T. Walker, J. Anal. At. Spectrom. 14 (1997) 447.
[19] J.L. Pouchou, F. Pichoir, La Recherche Aérospaciale 5 (1984) 167.
[20] C.T. Walker, J. Nucl. Mater. 80 (1979) 190.
[21] M. Coquerelle, P. Knappik, J.-C. Perrier, J. Phys. Paris 45 (C2) (1984) 84.
[22] K. Lassmann, C. O'Carroll, J. van de Laar, C.T. Walker, J. Nucl. Mater. 208 (1994) 223.
[23] C.T. Walker, T. Kameyama, S. Kitajima, M. Kinoshita, J. Nucl. Mater. 188 (1992) 73.
[24] A.H. Booth, A method for calculating fission gas diffusion from UO_2 and its application to the X-2-f loop test. Atomic Energy of Canada Ltd., Chalk River, Ontario Canada, Report AECL-496 (1957).
[25] Hj. Matzke, P.G. Lucuta, T. Wiss, Nucl. Instrun. Meth. B 166&167 (2000) 920.
[26] M. Mogensen, C. Bagger, C.T. Walker, J. Nucl. Mater. 199 (1993) 85.
[27] C. Bagger, M. Mogensen, C.T. Walker, J. Nucl. Mater. 211 (1994) 11.
[28] M. Mogensen, J.H. Pearce, C.T. Walker, J. Nucl. Mater. 264 (1999) 99.
[29] B. Sätmark, J.-P. Glatz, R. Malmbeck and C.T. Walker, 5th International Conference on Nuclear and Radiochemistry, Pontresina, Switzerland, 3–8 September 2000, Extended Abstracts, vol. 1, p. 247.
[30] J. Spino, D. Baron, M. Coquerelle, A.D. Stalios, J. Nucl. Mater. 256 (1998) 189.
[31] S. Bremier, R. Manzel, C.T. Walker, International Seminar on Fission Gas Behaviour in Water Reactor Fuels, Cadarache, France, 26–29 September 2000, NEA/NCS/DOC (2000) 20.
[32] S. Bremier, K. Lassman, C.T. Walker, Confirmation that fission gas release from recrystallised UO_2 grains in high burn-up water reactor fuel occurs by radiation-enhanced diffusion, The European Commission, Institute for Transuranium Elements, Karlsruhe, Germany, Report JRC-ITU-TN-2000/20 (2000).